Immobilization of Ionic Liquids to Covalent Organic Frameworks for Catalyzing Formylation of Amines with CO_2 and Phenylsilane

Bin Dong, Liangying Wang, Shang Zhao, Rile Ge, Xuedang Song, Yu Wang, Yanan Gao*

Dalian Institute of Chemical Physics, Chinese Academy of Sciences, 467 Zhongshan Road, Dalian 116023, China.

*Email: ygao@dicp.ac.cn; Fax: +86-411-84379992; Tel: +86-411-84379992.

Experimental section

Materials and methods

4,4′,4″,4‴-(Pyrene-1,3,6,8-tetrayl) tetraaniline (PyTTA)[S1] and 2,5-dihydroxyterephthalaldehyde (DHPA)[S2] were synthesized according to the reported procedures. Their ^1H NMR spectra matched well with those reported previously. 1,2-Dibromoethane, triethylamine, acetonitrile (CH_3CN), ethyl acetate (EtOAc), absolute alcohol, mesitylene, 1,4-dioxane, acetone, tetrahydrofuran (THF), acetic acid (AcOH), potassium carbonate (K_2CO_3), and anhydrous sodium sulfate (Na_2SO_4) were purchased from Shanghai Sinopharm Chemical Reagent Co., Ltd. Dehydrated *N*,*N*-dimethylformamide (DMF) were purchased from J&K Scientific Ltd. 1,4-Phthalaldehyde (PA), different kinds of amine substrates, and phenylsilane ($PhSiH_3$) were purchased from TCI. All reagents were used without further purification.

^1H NMR spectra were recorded on a Bruker Avance III 400 MHz spectrometer using tetramethylsilane as an internal standard. Powder X-ray diffraction (PXRD) data were measured on a PANalytical X’Pert Pro Multipurpose Diffractometer using Cu Kα radiation at 40 kV and 40 mA (step size: 0.017^{o}). Fourier transform infrared (FTIR) spectra were collected on a Bruker TENSOR 27 spectrometer. The ^{13}C cross-polarization magic-angle spinning (CP/MAS) solid-state NMR spectrum was recorded on a Varian Infinityplus-400 spectrometer with a $\pi/4$ pulse width of 1.5 μs, a contact time of 1 ms, a recycle delay of 2 s, and 64 scans. Elemental analysis was carried out on an Elementar Vario EL III elemental analyzer. The content of the bromide ions was determined by ion-chromatographic analyzer ICS-900 using the digested COFs. The thermal behavior was evaluated using a Netzsch STA 449 F3 thermal analyzer under a nitrogen atmosphere with a heating rate of 10 ^{o}C/min. All gas sorption experiments were collected using a Quantachrome Autosorb-iQ2 analyzer with ultra-high-purity gases. The fresh sample was activated at 100 °C for 10 h under high-vacuum conditions prior to analysis to make the pores guest-free.

To obtain the isosteric heat of adsorption (Q_{st}), the adsorption data at 273 and 298

K were modeled with virial-type expression composed of parameters a_i and b_i that are independent of temperature.[S3-S5] In each case, the data were fitted using the equation:

$$lnP = lnN + \frac{1}{T}\sum_{i=0}^{m} a_i N^i + \sum_{i=0}^{n} b_i N^i$$

Here, P is pressure expressed in torr; N is the adsorption capacity expressed in mmol/g; T is the absolute temperature expressed in K; and m and n determine the number of terms required to adequately describe the isotherm. Successive terms were included in the fitting expression until and the average value of the squared deviations from the experimental values was minimized, usually $m \leq 6$ and $n \leq 3$. The values of the virial coefficients a_0 to a_m were then used to calculate Q_{st} through the following expression:

$$Q_{st} = -R\sum_{i=0}^{m} a_i N^i$$

Where R is the universal gas constant.

Synthetic procedures

(2-bromoethyl)triethylammonium bromide ([BrEtEt$_3$N]Br). A solution of triethylamine (1.0 g, 9.9 mmol) and 1,2-dibromoethane (9.3 g, 49.4 mmol) in CH_3CN (50 mL) was refluxed for 4 h.[S6] After cooled to room temperature the solvent was removed. The resulting residue was dissolved in hot CH_3CN. Cooling of this solution gave precipitates which were mostly the dicationic product. The precipitates were removed by filtration. Added EtOAc to the filtrate, white solids appeared, which were isolated by filtration and dried under vacuum to give (2-bromoethyl)triethylammonium bromide ([BrEtEt$_3$N]Br) (0.61 g, 21% yield). ^{1}H NMR ($CDCl_3$): δ (ppm) = 3.88 (t, 2H), 3.77 (t, 2H), 3.65 (q, 6H), 1.39 (s, 9H); ^{13}C NMR ($CDCl_3$): δ (ppm) = 58.0, 54.2, 21.8, 8.3.

[HO]$_{X\%}$-Py-COFs. PyTTA (11.3 mg, 0.02 mmol) and DHPA/PA (total 0.04 mmol) at different molar ratios of 0/100, 10/90, 25/75, 50/50, 75/25, and 100/0 were weighed into a glass ampoule (ca. 5 mL), which were suspended in mesitylene (0.5 mL) and 1,4-dioxane (0.5 mL) with 0.1 mL of 6 M AcOH.[S7] After sonicated for 10 min, the ampoule was degassed by three freeze-pump-thaw cycles and then flame-sealed.

Upon warming to room temperature, the ampoule was placed in an oven at 120 ºC and left undisturbed for 3 days, yielding solids along the tube. The ampoule was broken at the neck and the solids was isolated by filtration, washed with THF and acetone, and finally dried at 100 ºC under vacuum for 12 h to give the corresponding COFs in isolated yields of 86%, 87%, 90%, 84%, and 90% for [HO]$_{0\%}$-Py-COF, [HO]$_{25\%}$-Py-COF, [HO]$_{50\%}$-Py-COF, [HO]$_{75\%}$-Py-COF, and [HO]$_{100\%}$-Py-COF, respectively.

[Et$_4$NBr]$_{50\%}$-Py-COF. A mixture of [HO]$_{50\%}$-Py-COF (30 mg), [BrEtEt$_3$N]Br (30 mg), and K_2CO_3 (21 mg) in dry DMF (5 mL) was stirred at reflux for 24 h.[S8] After cooling, the precipitate was collected by filtration, washed with EtOH and acetone, and then dried at 100 ºC under vacuum for 12 h to give [Et$_4$NBr]$_{50\%}$-Py-COF quantitatively as a dark red solid. The similar reaction procedure was used to prepare other [Et$_4$NBr]$_{X\%}$-Py-COFs from [HO]$_{X\%}$-Py-COFs ($X = 25, 75, 100$).

Formamide derivatives. [Et$_4$NBr]$_{50\%}$-Py-COF (18 mg) was transferred into a dry three-neck flask already connected to a CO_2 balloon. After three vacuum and CO_2–purge cycles, amine (1 mmol), $PhSiH_3$ (2 mmol), and dry DMF (1 mL) were introduced into the flask. The flask was stirred at 30 ºC for 24 h. After that, EtOAc was added to the mixture and aqueous work up was performed. The combined organic phase was dried with anhydrous Na_2SO_4 and the product was purified by column chromatography using EtOAc/hexane (1:2) to give corresponding formamides.

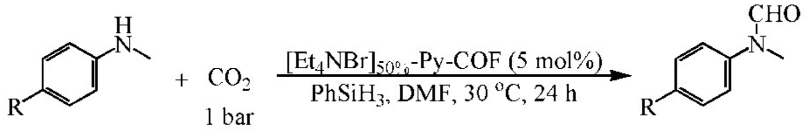

1 **2**

N-methylformanilide (**2a**, 94% yield): ^{1}H NMR ($CDCl_3$): δ (ppm) = 8.46 (s, 1H), 7.39–7.43 (m, 2H), 7.27–7.29 (m 1H), 7.14–7.17 (m, 2H), 3.31 (s, 3H); ^{13}C NMR ($CDCl_3$): δ (ppm) = 162.5, 142.3, 129.7, 126.5, 122.5, 32.2.

N,4′-dimethylformanilide (**2b**, 91% yield): ^{1}H NMR ($CDCl_3$): δ (ppm) = 8.42 (s, 1H), 7.22 (d, 2H), 7.07 (d, 2H), 3.29 (s, 3H), 2.36 (s, 3H); ^{13}C NMR ($CDCl_3$): δ (ppm) = 162.5, 139.8, 136.5, 130.3, 122.7, 32.4, 20.9.

N-methyl-4-methoxylformanilde (**2c**, 92% yield): ^{1}H NMR ($CDCl_3$): δ (ppm) = 8.32

(s, 1H), 7.09 (d, 2H), 6.93 (d, 2H), 3.81 (s, 3H), 3.25 (s, 3H); ^{13}C NMR ($CDCl_3$): δ (ppm) = 162.6, 158.4, 135.4, 124.8, 114.9, 55.7, 32.8.

N-(4-chlorophenyl)-*N*-methylformamide (**2d**, 92% yield): ^{1}H NMR ($CDCl_3$): δ (ppm) = 8.42 (s, 1H), 7.38 (d, 2H), 7.10 (d, 2H), 3.28 (s, 3H); ^{13}C NMR ($CDCl_3$): δ (ppm) = 162.2, 140.8, 132.2, 129.9, 123.7, 32.2.

N-(4-fluorophenyl)-*N*-methylformamide (**2e**, 88% yield): ^{1}H NMR ($CDCl_3$): δ (ppm) = 8.37 (s, 1H), 7.08-7.15 (m, 4H), 3.28 (s, 3H); ^{13}C NMR ($CDCl_3$): δ (ppm) = 162.4, 124.8, 124.7, 116.8, 116.5, 32.6.

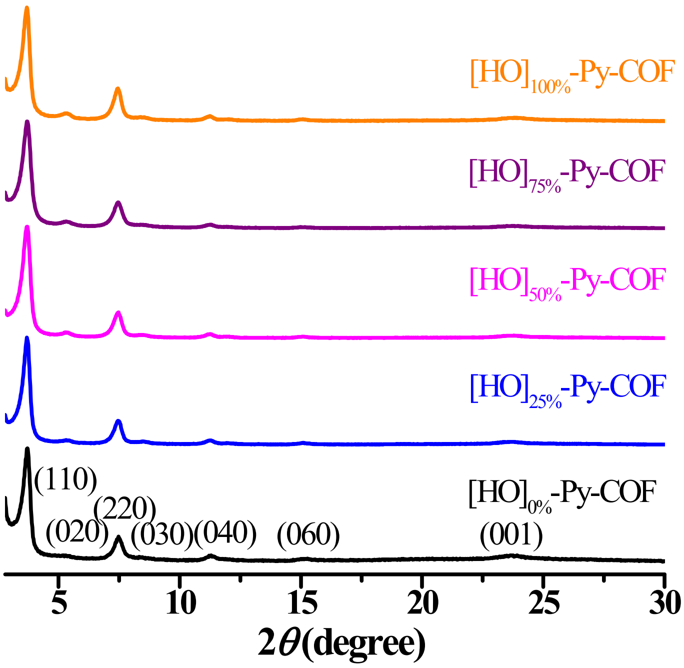

Fig. S1 PXRD patterns of $[HO]_{X\%}$-Py-COFs (X = 0, 25, 50, 75, 100). Without hydroxyl groups in phenyl rings, PA with PyTTA constructed a new COF material ($[HO]_{0\%}$-Py-COF) with well-defined crystalline structures. DHPA/PA at different molar ratios (X = 25, 50, 75) with PyTTA all produced COF materials with structures similar to $[HO]_{0\%}$-Py-COF and $[HO]_{100\%}$-Py-COF.

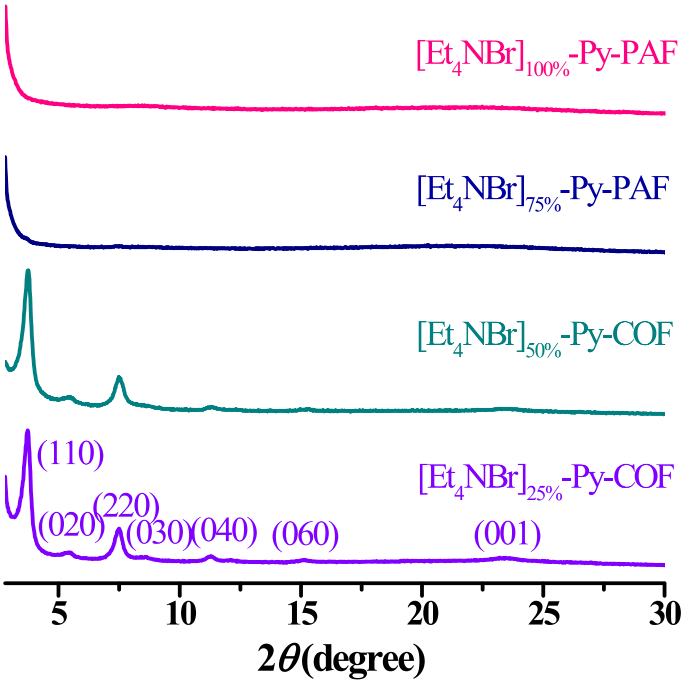

Fig. S2 PXRD patterns of [Et$_4$NBr]$_{X\%}$-Py-COFs (X = 25, 50) and [Et$_4$NBr]$_{X\%}$-Py-PAFs (X = 75, 100). With the increase of hydroxyl groups in [HO]$_{X\%}$-Py-COFs, the corresponding ionic materials had no crystalline structures but yielded amorphous materials ([Et$_4$NBr]$_{75\%}$-Py-PAF and [Et$_4$NBr]$_{100\%}$-Py-PAF). In other words, the crystal structures were only retained after modification when the ionization degree on the channel walls was moderate. The following examinations were focused on the COF materials unless otherwise stated.

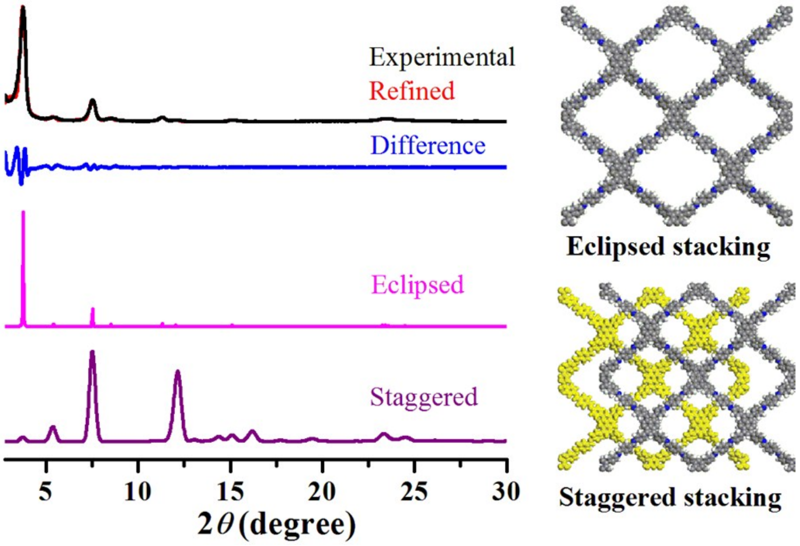

Fig. S3 PXRD patterns of $[HO]_{0\%}$-Py-COF: experimental (black), refined (red), the difference (blue, experimental minus refined profiles), and simulated patterns using eclipsed AA stacking mode (magenta), and the simulated pattern using staggered AB stacking mode (purple).

Table S1 Elemental analysis data of the COFs.

Py-COFs		C%	H%	N%
$[HO]_{0\%}$	Calcd.	88.16	4.49	7.34
	Found	84.36	4.78	6.59
$[HO]_{25\%}$	Calcd.	86.35	4.40	7.19
	Found	84.01	4.32	6.84
$[HO]_{50\%}$	Calcd.	84.61	4.31	7.05
	Found	82.34	4.45	6.58
$[HO]_{75\%}$	Calcd.	82.95	4.23	6.91
	Found	81.20	4.36	6.30
$[HO]_{100\%}$	Calcd.	81.34	4.14	6.78
	Found	79.42	4.35	6.01
$[Et_4NBr]_{25\%}$	Calcd.	77.88	5.31	7.10
	Found	75.53	4.53	6.39
$[Et_4NBr]_{50\%}$	Calcd.	71.40	5.83	6.94
	Found	73.98	4.72	6.26

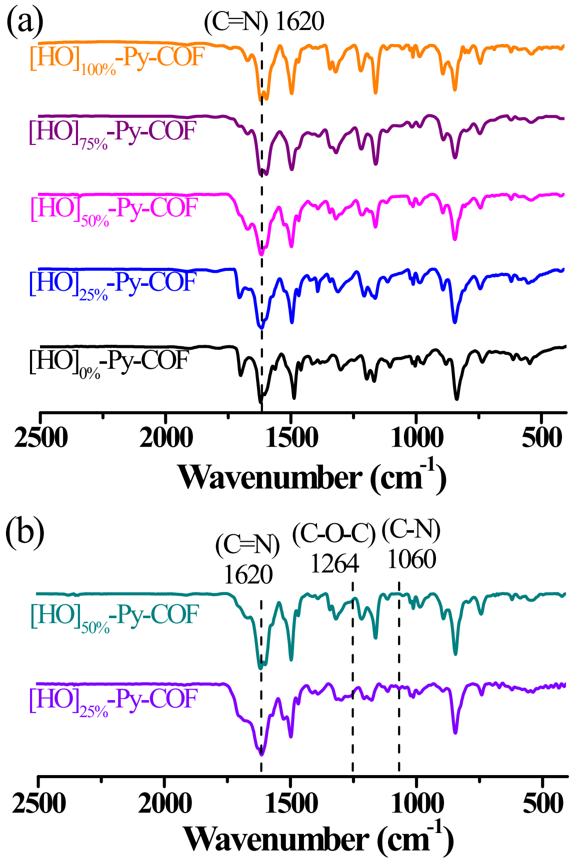

Fig. S4 FTIR spectra of (a) [HO]$_{X\%}$-Py-COFs (X = 0, 25, 50, 75, 100) and (b) [Et$_4$NBr]$_{X\%}$-Py-COFs (X = 25, 50). The appearance of an intensive band around 1620 cm^{-1} in [HO]$_{X\%}$-Py-COFs confirmed the formation of an imine bond. After the functionalization, the C=N bands were remained, suggesting that the frameworks are still stable. As for [Et$_4$NBr]$_{X\%}$-Py-COFs, several new peaks appeared at 1264 and 1060 cm^{-1}, which was assigned to the C-O-C and C-N stretching bands, respectively, indicating that the ionic liquid groups were grafted onto the channel walls of the COFs.

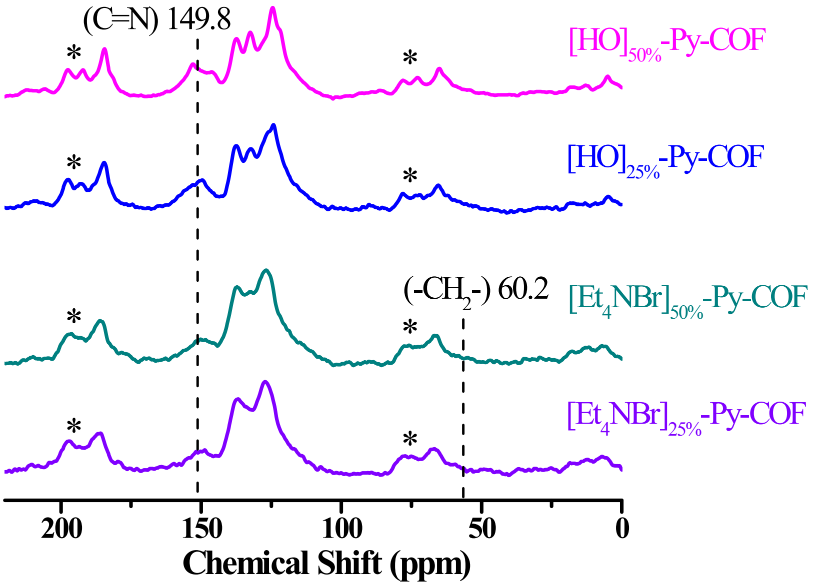

Fig. S5 Solid-state ^{13}C CP/MAS NMR spectra of $[HO]_{X\%}$-Py-COFs and $[Et_4NBr]_{X\%}$-Py-COFs (X = 25, 50). Signals with * are side bands. A peak at 149.8 ppm arised from the C=N bond, which confirmed that the crystalline imine-linked structures were retained after functionalization. Comapred with $[HO]_{X\%}$-Py-COFs, a new signal (not so evident) appeared at 60.2 ppm assigned to the $-CH_2-$ bond in $[Et_4NBr]_{X\%}$-Py-COFs, suggesting the ionic liquid units grafted onto the channel walls of the COFs.

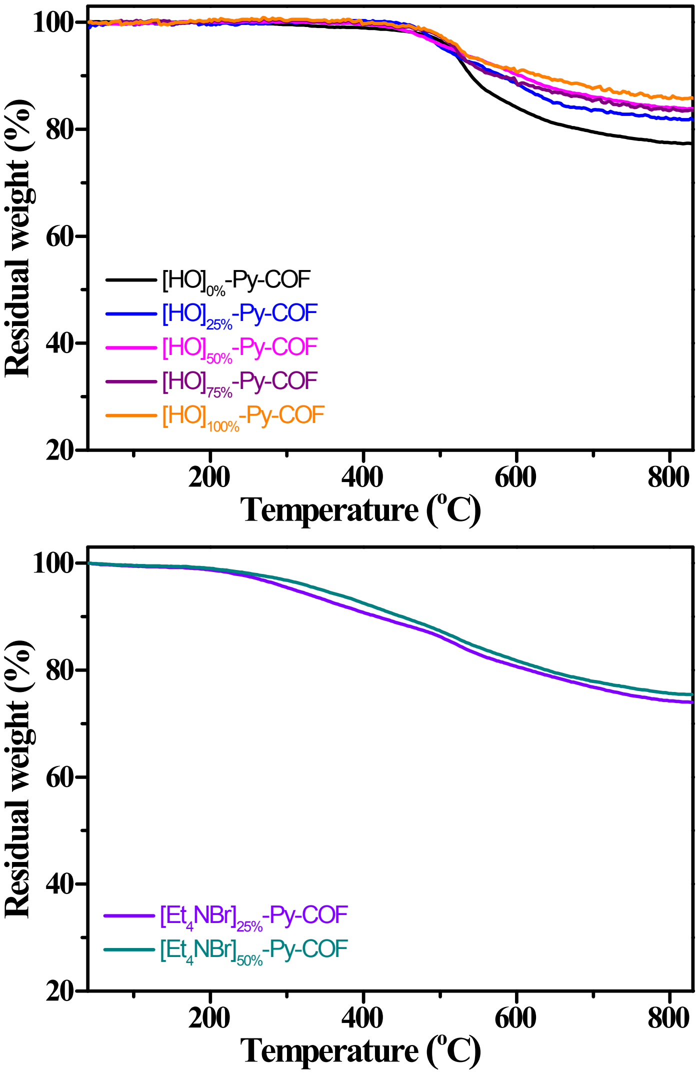

Fig. S6 TGA data of (a) [HO]$_{X\%}$-Py-COFs (X = 0, 25, 50, 75, 100) and (b) [Et$_4$NBr]$_{X\%}$-Py-COFs (X = 25, 50) under a nitrogen atmosphere. As for [Et$_4$NBr]$_{X\%}$-Py-COFs (X = 25, 50), the weight loss around 300 °C was due to the decomposition of the linear chains on the channel walls.

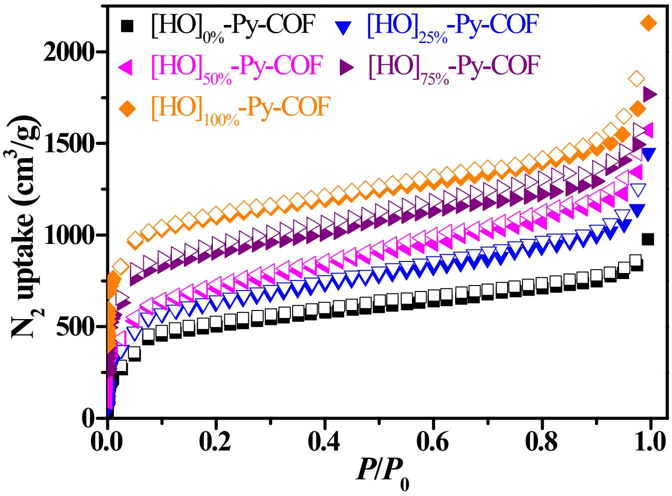

Fig. S7 N_2 sorption isotherms of $[HO]_{X\%}$-Py-COFs ($X = 0, 25, 50, 75, 100$). Except $[HO]_{0\%}$-Py-COFs, the nitrogen sorption isotherms of other COFs were drawn by shifting the N_2 uptake values appropriately.

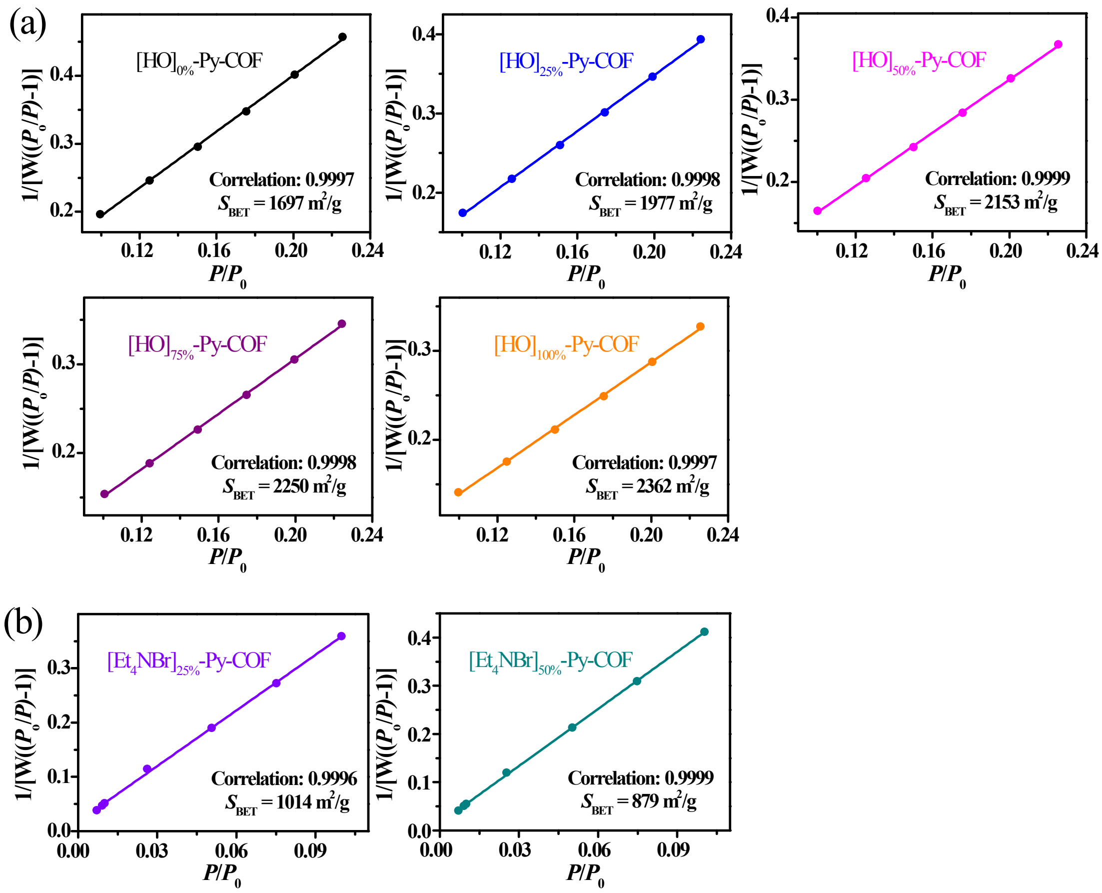

Fig. S8 BET surface area plots of (a) [HO]$_{X\%}$-Py-COFs (X = 0, 25, 50, 75, 100) and (b) [Et$_4$NBr]$_{X\%}$-Py-COFs (X = 25, 50) calculated from the N_2 adsorption isotherm at 77 K.

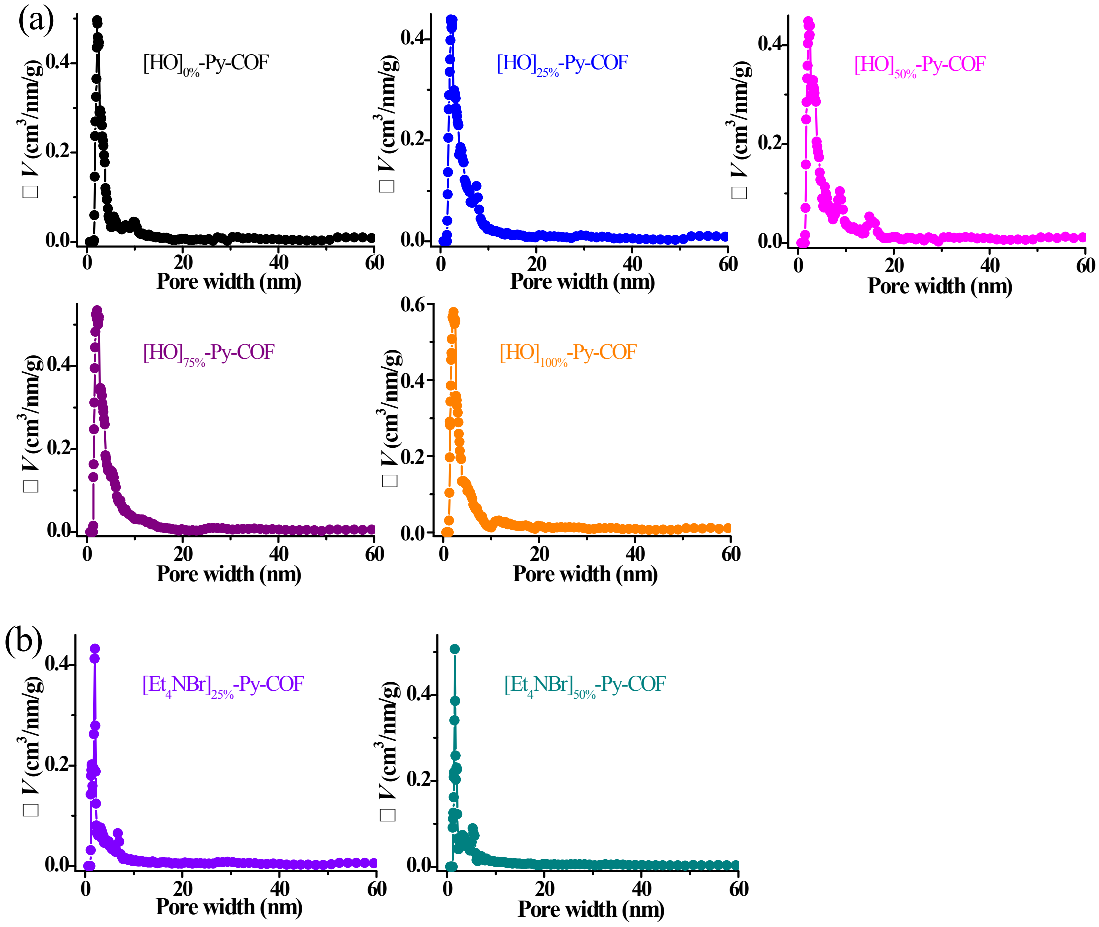

Fig. S9 Pore size distribution curves by fitting NLDFT to the N_2 adsorption data at 77 K of $[HO]_{X\%}$-Py-COFs ($X = 0, 25, 50, 75, 100$) and $[Et_4NBr]_{X\%}$-Py-COFs ($X = 25, 50$).

Table S2 Pore parameters of $[HO]_{X\%}$-Py-COFs (X = 0, 25, 50, 75, 100) and

$[Et_4NBr]_{X\%}$-Py-COFs (X = 25, 50).

Py-COFs	S_{BET} (m^2/g)	Pore width (nm)	Pore volume (cm^3/g)
$[HO]_{0\%}$	1697	2.2	1.51
$[HO]_{25\%}$	1977	2.2	2.16
$[HO]_{50\%}$	2153	2.2	2.29
$[HO]_{75\%}$	2250	2.2	2.35
$[HO]_{100\%}$	2362	2.2	2.72
$[Et_4NBr]_{25\%}$	1014	2.0	1.05
$[Et_4NBr]_{50\%}$	879	1.6	0.99

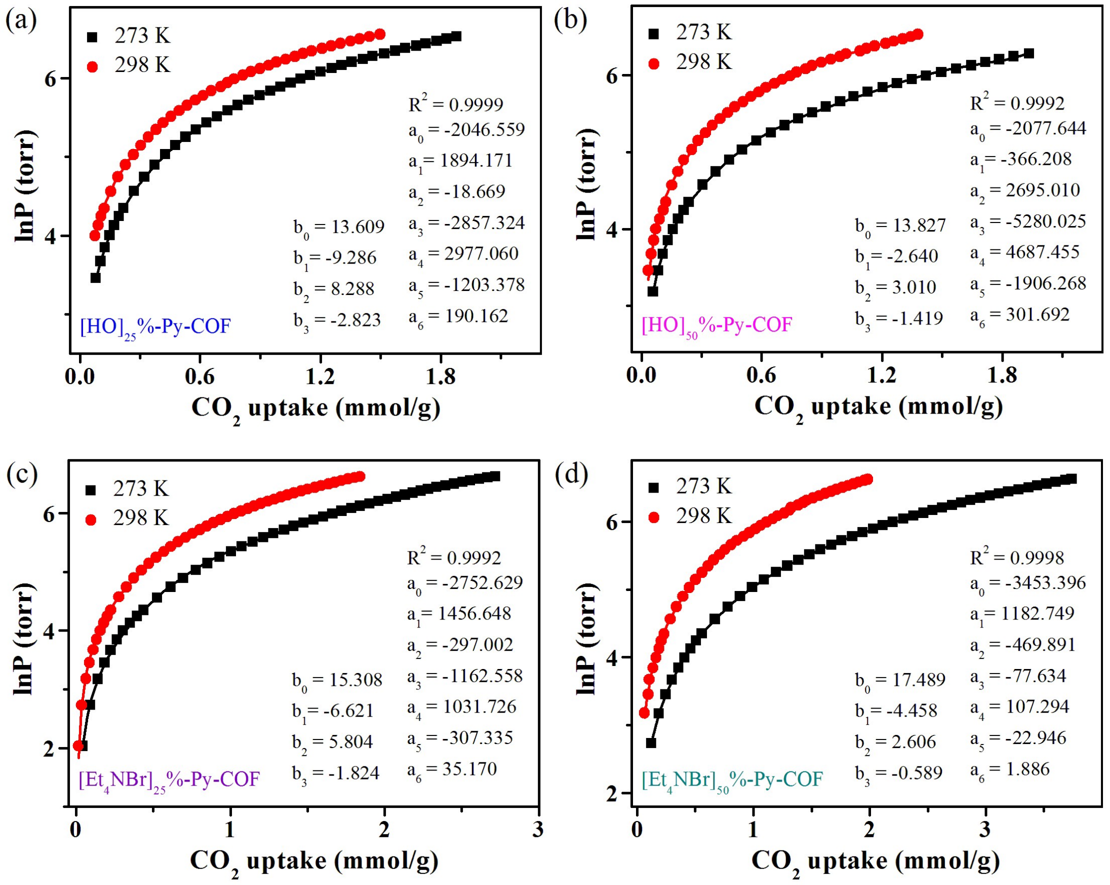

Fig. S10 CO_2 adsorption isotherms at 273 and 298 K (symbol) and the virial equation fits (line) for (a) $[HO]_{25\%}$-Py-COF, (b) $[HO]_{50\%}$-Py-COF, (c) $[Et_4NBr]_{25\%}$-Py-COF, and (d) $[Et_4NBr]_{50\%}$-Py-COF.

Table S3 CO_2 uptake and Q_{st} for CO_2 of $[HO]_{X\%}$-Py-COFs and $[Et_4NBr]_{X\%}$-Py-COFs ($X = 25, 50$).

Py-COFs	CO_2 uptake[a] (mg/g)	Q_{st} for CO_2[b] (kJ/mol)
$[HO]_{25\%}$	91.7 (72.4)	16.9
$[HO]_{50\%}$	114.2 (68.6)	17.3
$[Et_4NBr]_{25\%}$	119.6 (80.9)	22.9
$[Et_4NBr]_{50\%}$	164.6 (87.3)	28.7

[a] Calculated at 1 bar under 273 and 298 K (in parenthesis). [b] At zero coverage calculated using the virial method.

Table S4 Summary of CO_2 uptake (at 1 bar) and Q_{st} for CO_2 of the reported COFs.

COFs	CO_2 uptake[a] (mg/g)	Q_{st} for CO_2 (kJ/mol)
COF-5[S9]	59	–
COF-103[S9]	76	–
TDCOF-5[S10]	92	21.8
ILCOF-1[S11]	60 (32)	18.3
TH-COF-1[S12]	128	31
ACOF-1[S13]	177	27.6
AB-COF (ACOF-1) [S14]	149	29.7
COF-JLU2[S15]	217	31
ATFG-COF (COF-JLU2)[S14]	173	33.3
TpPa-COF (MW)[S16]	218	34.1
TAPB-TFPB[S17]	40	–
iPrTAPB-TFPB[S17]	31	–
TAPB-TFP[S17]	180	–
iPrTAPB-TFP[S17]	105	–
TAT-COF-2[S18]	77	–
$[HO]_{100\%}$-H_2P-COF[S19]	63	36.4
$[HO_2C]_{100\%}$-H_2P-COF[S19]	174	43.5
$[AcOH]_{50}$-H_2P-COF[S20]	117	17.8
$[EtOH]_{50}$-H_2P-COF[S20]	124	19.7
$[EtNH_2]_{50}$-H_2P-COF[S20]	157	20.9
N-COF[S21]	120 (64)[b]	–
$[HO]_{50\%}$-Py-COF[c]	114 (69)	17.3
$[Et_4NBr]_{50\%}$-Py-COF[c]	165 (87)	28.7

[a]Measured under 273 and 298 K (in parenthesis). [b]At 1 atm. [c]COFs in this work.

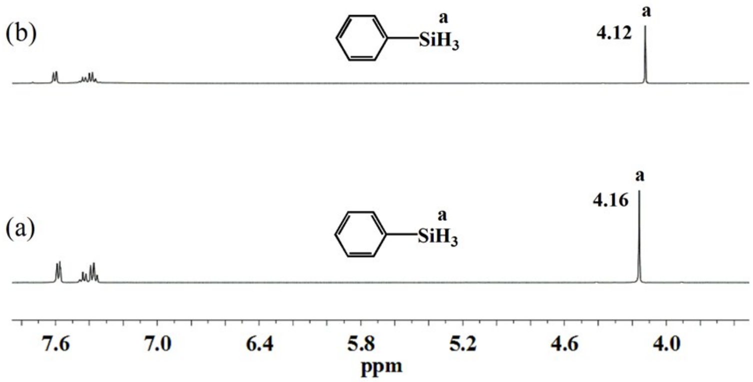

Fig. S11 ^{1}H NMR spectra (DMSO-d6) of (a) $PhSiH_3$ and (b) its mixture with $[Et_4NBr]_{50\%}$-Py-COF in DMF. The signal assigning to Si-H of phenylsilane shifted from 4.16 to 4.12 ppm, demonstrating the interaction between $PhSiH_3$ and $[Et_4NBr]_{50\%}$-Py-COF. The $[Et_4NBr]_{50\%}$-Py-COF activated the Si-H bond of phenylsilane, which may make it more favorable for the insertion of CO_2.[S22]

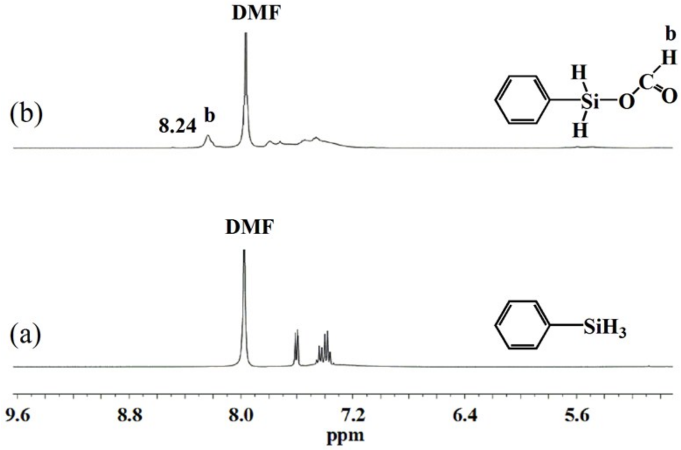

Fig. S12 ^{1}H NMR spectra (DMSO-d6) of (a) the mixture of $PhSiH_3$ and $[Et_4NBr]_{50\%}$-Py-COF in DMF and (b) the same mixture under 1 bar CO_2 after stirred for 12 h and CO_2 release. In Fig. S12b, a new signal appeared at 8.24 ppm ascribed to formoxysilane, which suggested that the reaction between $PhSiH_3$ and CO_2 occured catalyzed by $[Et_4NBr]_{50\%}$-Py-COF.

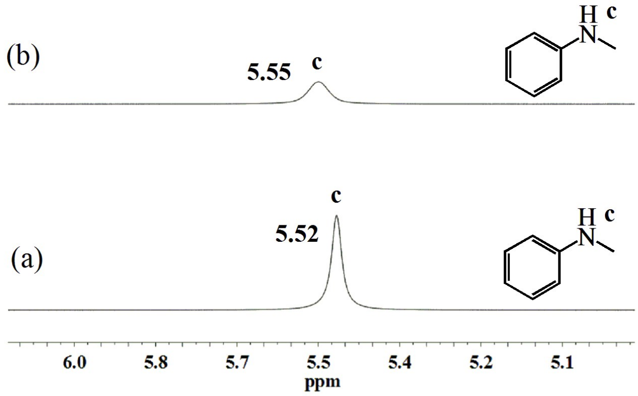

Fig. S13 ^{1}H NMR spectra (DMSO-d6) of (a) *N*-methylaniline and (b) the mixture with $[Et_4NBr]_{50\%}$-Py-COF in DMF. The chemical shift of N-H in amine was observed, probably due to the hydrogen bond between the amine and bromide ion of $[Et_4NBr]_{50\%}$-Py-COF.

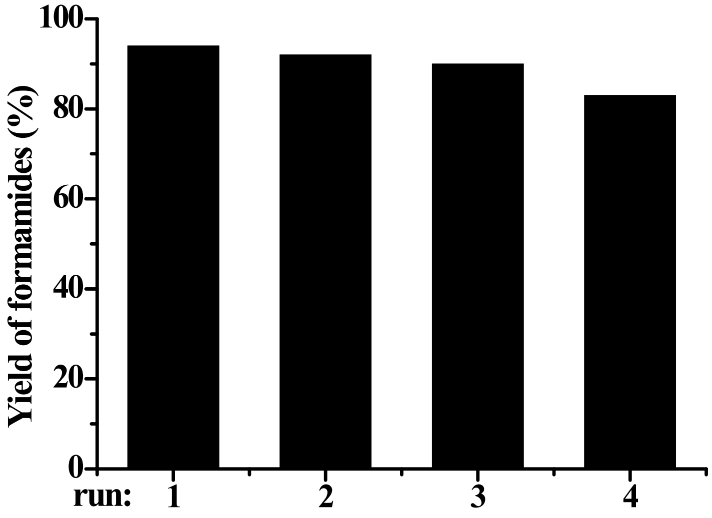

Fig. S14 Reuse of the $[Et_4NBr]_{50\%}$-Py-COF catalyst. Reaction conditions: 1 mmol of **1a**, 2 mmol of $PhSiH_3$, 1mL of DMF, initial pressure of CO_2 at 1 bar, 30 ºC, 24 h.

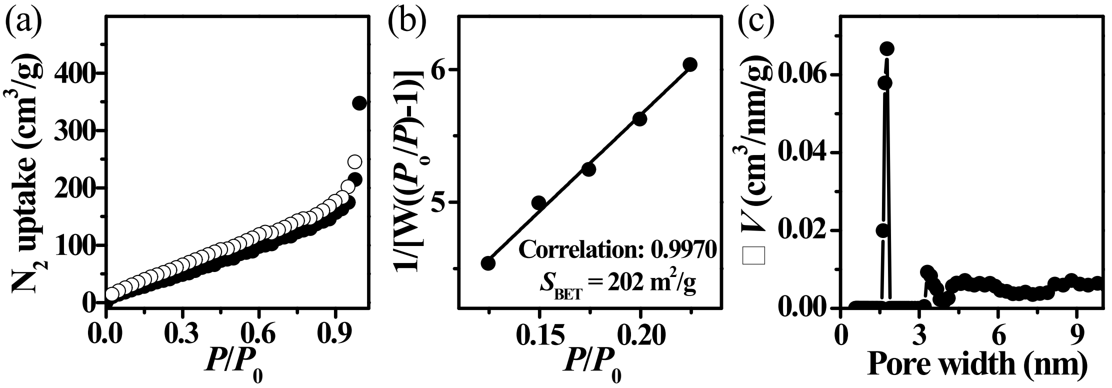

Fig. S15 (a) N_2 sorption isotherms measured at 77 K, (b) BET surface area plot, and (c) pore size distribution of the $[Et_4NBr]_{50\%}$-Py-COF after the fourth cycle.

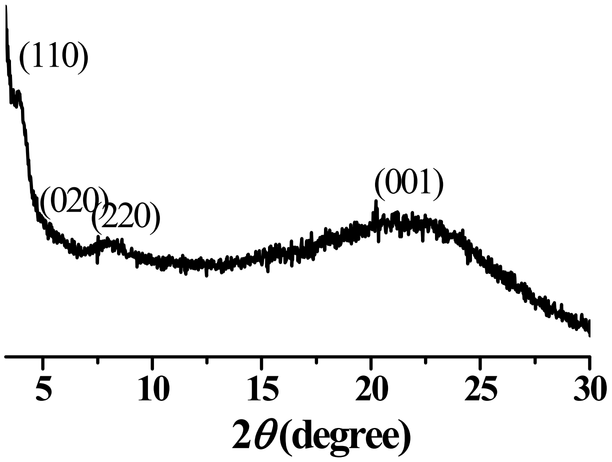

Fig. S16 The PXRD pattern of of the $[Et_4NBr]_{50\%}$-Py-COF after the fourth cycle.

Reference

S1 S. Jin, T. Sakurai, T. Kowalczyk, S. Dalapati, F. Xu, H. Wei, X. Chen, J. Gao, S. Seki, S. Irle and D. Jiang, *Chem. Eur. J.*, 2014, **20**, 14608–14613.

S2 T. Kretz, J. W. Bats, H.-W. Lerner and M. Wagner, *Z. Naturforsch.*, 2007, **62b**, 66–74.

S3 J. L. C. Rowsell and O. M. Yaghi, *J. Am. Chem. Soc.*, **2006**, *128*, 1304–1315.

S4 B. Zheng, J. Bai, J. Duan, L. Wojtas and M. J. Zaworotko, *J. Am. Chem. Soc.*, 2011, **133**, 748–751.

S5 B. X. Dong, S. Y. Zhang, W. L. Liu, Y. C. Wu, J. Ge, L. Song and Y. L. Teng, *Chem. Commun.*, 2015, **51**, 5691–5694.

S6 W. Yang, P. S. Chan, M. S. Chan, K. F. Li, P. K. Lo, N. K. Mak, K. W. Cheah, M. S. Wong, *Chem. Commun.*, 2013, **49**, 3428–3430.

S7 X. Chen, N. Huang, J. Gao, H. Xu, F. Xu and D. Jiang, *Chem. Rev.*, 2014, **50**, 6161–6163.

S8 H. Maeda, Y. Haketa and T. Nakanishi, *J. Am. Chem. Soc.*, 2007, **129**, 13661–13674.

S9 H. Furukawa and O. M. Yaghi, *J. Am. Chem. Soc.*, **2009**, *131*, 8875–8883.

S10 Z. Kahveci, T. Islamoglu, G. A. Shar, R. Ding and H. M. El-Kaderi, *CrystEngComm*, **2013**, *15*, 1524–1527.

S11 M. G. Rabbani, A. K. Sekizkardes, Z. Kahveci, T. E. Reich, R. Ding and H. M. El-Kaderi, *Chem. Eur. J.*, **2013**, *19*, 3324–3328.

S12 L. Wang, B. Dong, R. Ge, F. Jiang, J. Xiong, Y. Gao and J. Xu, *Micropor. Mesopor. Mat.*, **2016**, *224*, 95–99.

S13 Z. Li, X. Feng, Y. Zou, Y. Zhang, H. Xia, X. Liu and Y. Mu, *Chem. Commun.*, **2014**, *50*, 13825–13828.

S14 L. Stegbauer, M. W. Hahn, A. Jentys, G. Savasci, C. Ochsenfeld, J. A. Lercher and B. V. Lotsch, *Chem. Mater.*, **2015**, *27*, 7874–7881.

S15 Z. Li, Y. Zhi, X. Feng, X. Ding, Y. Zou, X. Liu and Y. Mu, *Chem. Eur. J.*, **2015**, *21*, 12079–12084.

S16 H. Wei, S. Chai, N. Hu, Z. Yang, L. Wei and L. Wang, *Chem. Commun.*, **2015**, *51*, 12178–12181.

S17 D. Kaleeswaran, P. Vishnoi and R. Murugavel, *J. Mater. Chem. C*, **2015**, *3*, 7159–7171.

S18 Y.-F. Xie, S.-Y. Ding, J.-M. Liu, W. Wang and Q.-Y. Zheng, *J. Mater. Chem. C*, **2015**, *3*, 10066–10069.

S19 N. Huang, X. Chen, R. Krishna and D. Jiang, *Angew. Chem. Int. Ed.*, **2015**, *54*, 2986–2990.

S20 N. Huang, R. Krishna and D. Jiang, *J. Am. Chem. Soc.*, **2015**, *137*, 7079–7082.

S21 Q. Gao, L. Bai, X. Zhang, P. Wang, P. Li, Y. Zeng, R. Zou and Y. Zhao, *Chin. J. Chem.*, **2015**, *33*, 90–94.

S22 L. Hao, Y. Zhao, B. Yu, Z. Yang, H. Zhang, B. Han, X. Gao and Z. Liu, *ACS Catal.*, 2015, **5**, 4989–4993.

^{1}H and ^{13}C NMR Spectra

(2-bromoethyl)triethylammonium bromide ([BrEtEt$_3$N]Br)

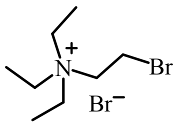

^{1}H NMR in $CDCl_3$

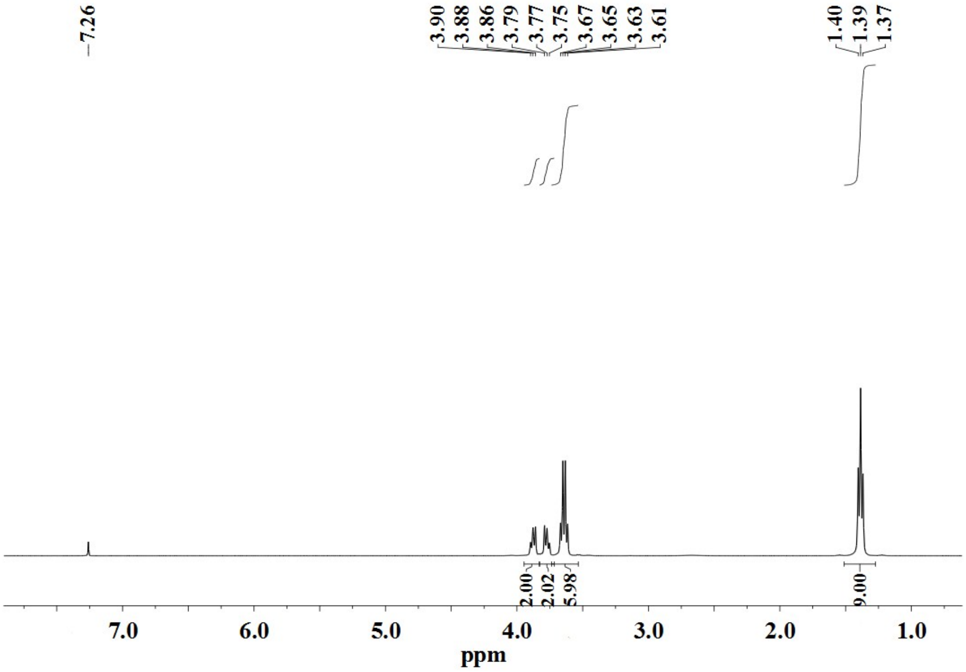

^{13}C NMR in $CDCl_3$

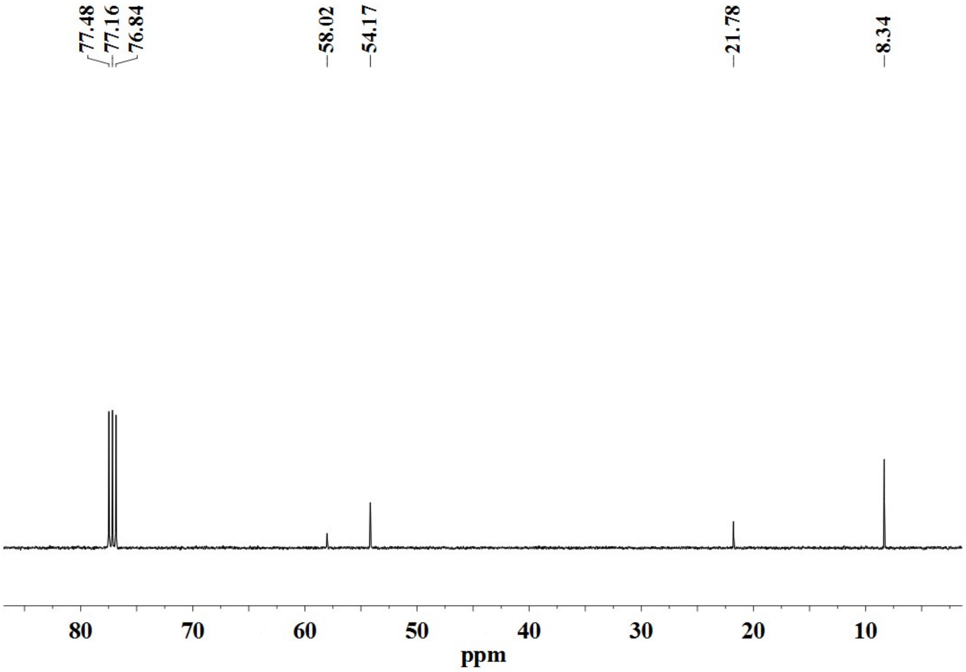

N-methylformanilide (**2a**)

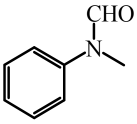

^{1}H NMR in $CDCl_3$

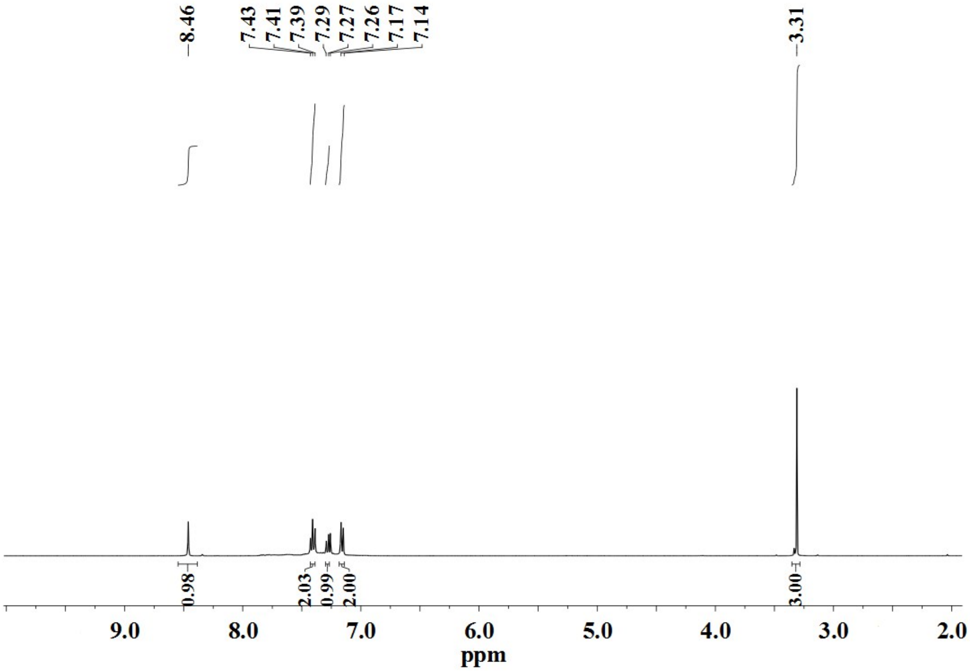

^{13}C NMR in $CDCl_3$

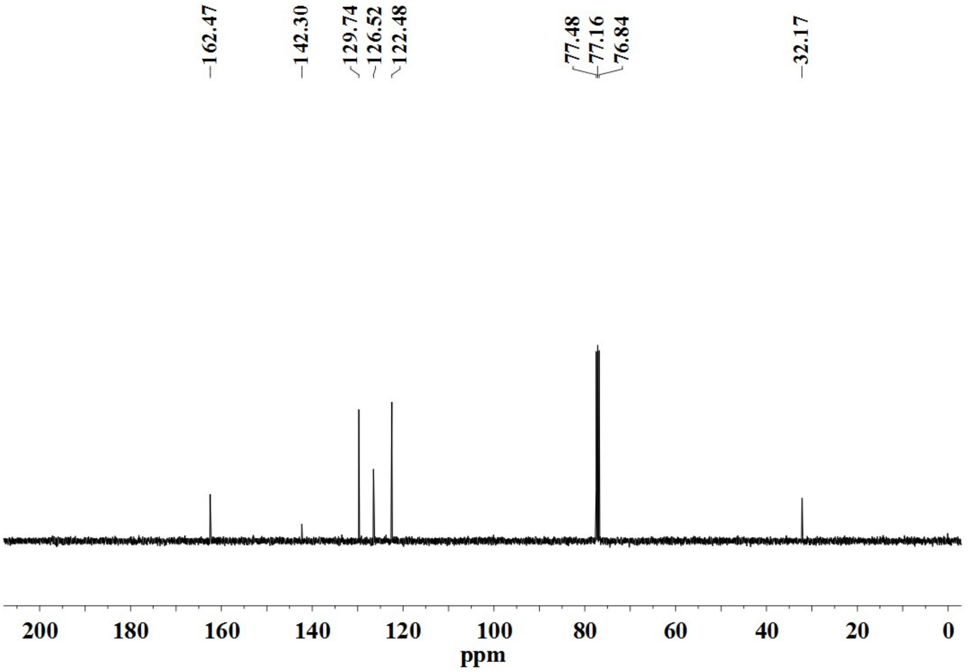

N,4′-dimethylformanilide (**2b**)

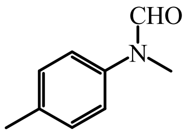

^{1}H NMR in $CDCl_3$

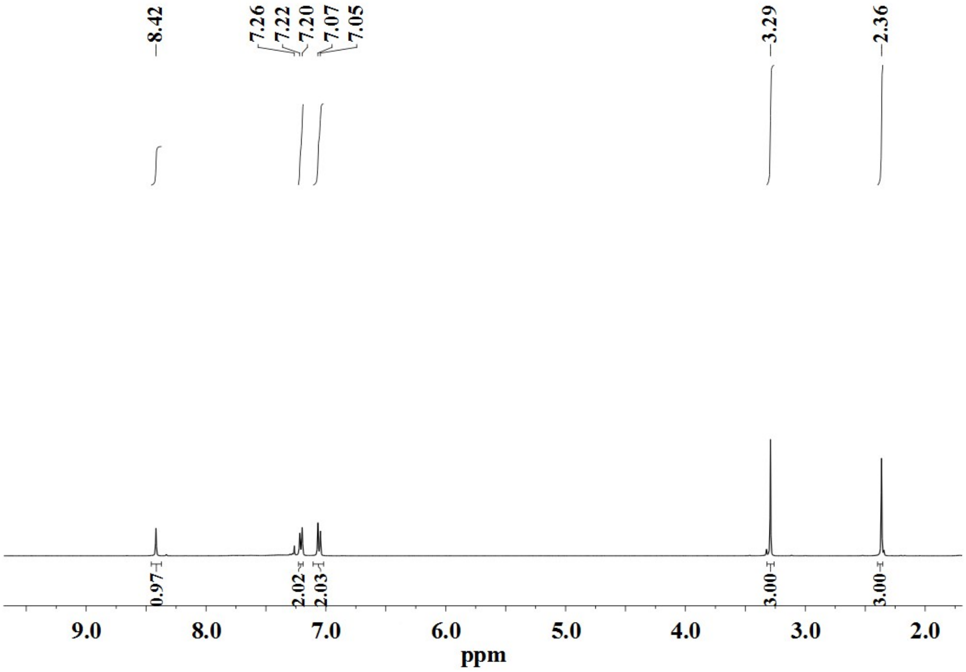

^{13}C NMR in $CDCl_3$

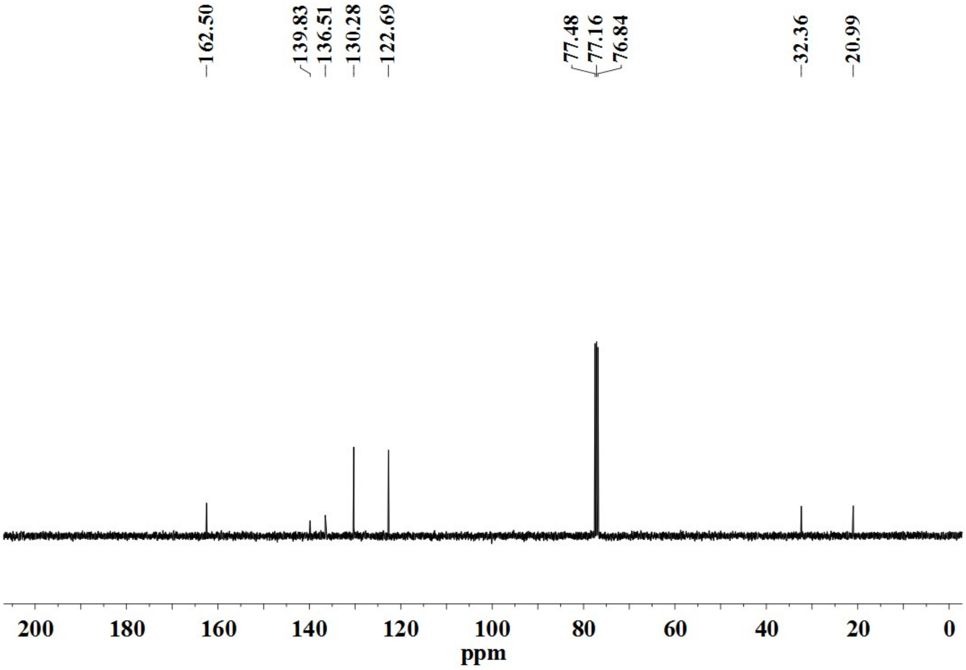

N-methyl-4-methoxylformanilde (**2c**)

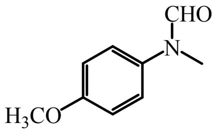

^{1}H NMR in CDCl$_3$

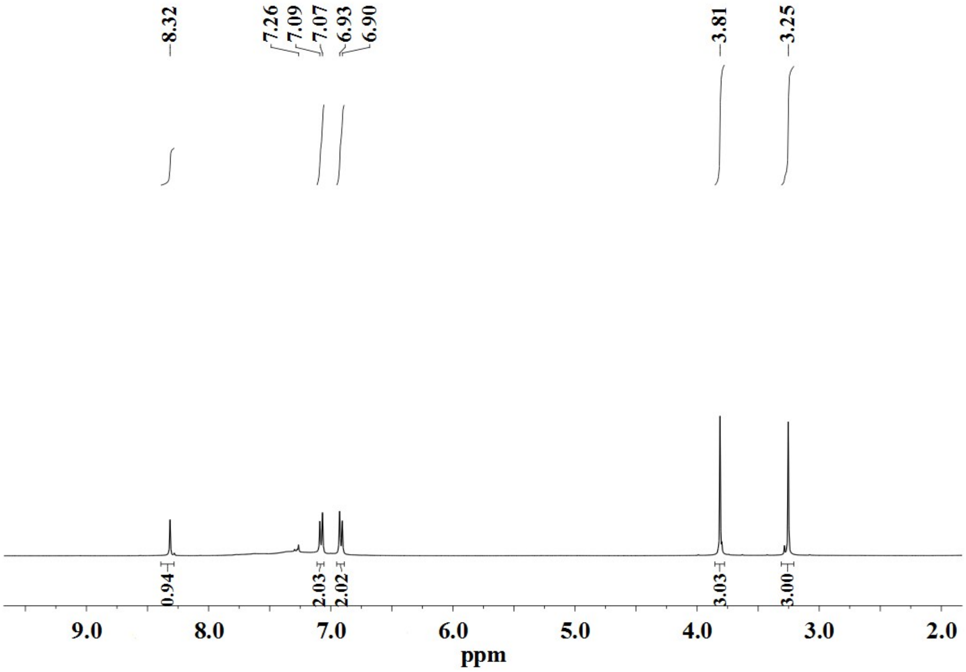

^{13}C NMR in CDCl$_3$

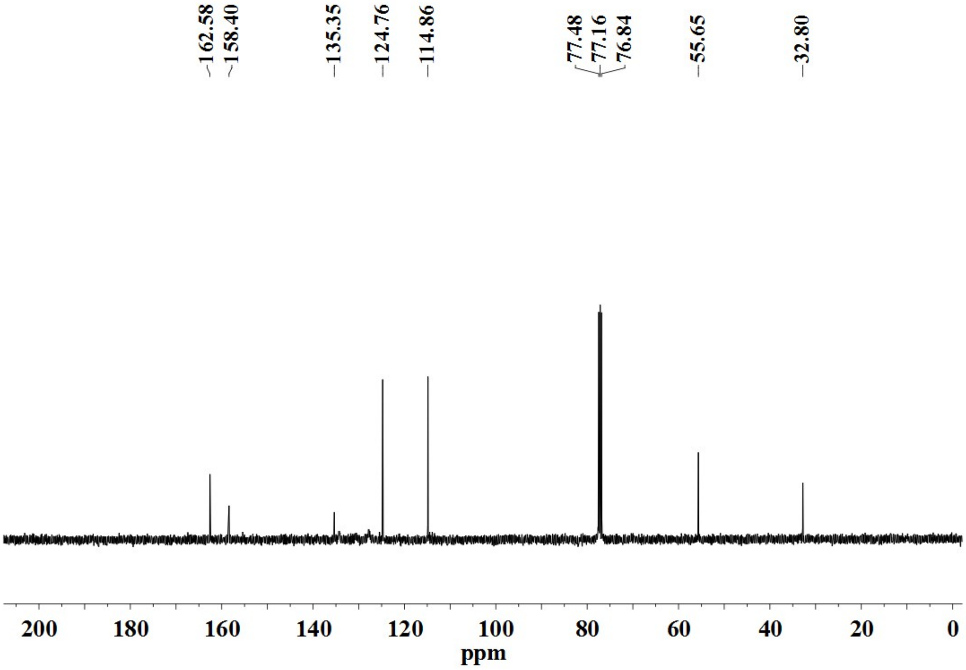

N-(4-chlorophenyl)-*N*-methylformamide (**2d**)

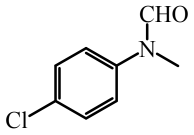

^{1}H NMR in $CDCl_3$

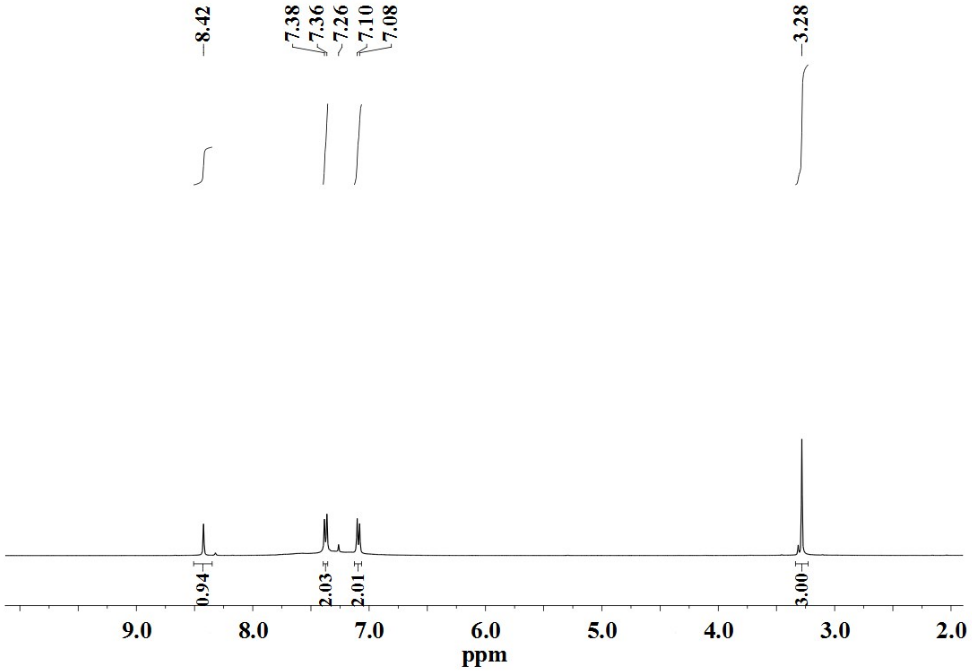

^{13}C NMR in $CDCl_3$

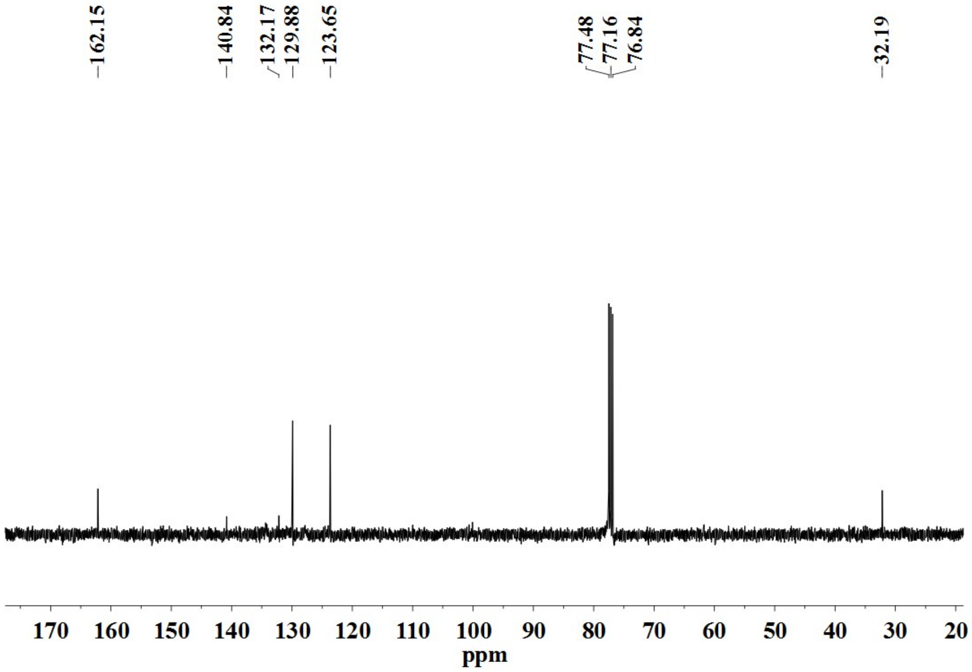

N-(4-fluorophenyl)-*N*-methylformamide (**2e**)

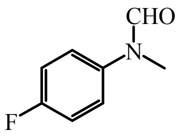

^{1}H NMR in $CDCl_3$

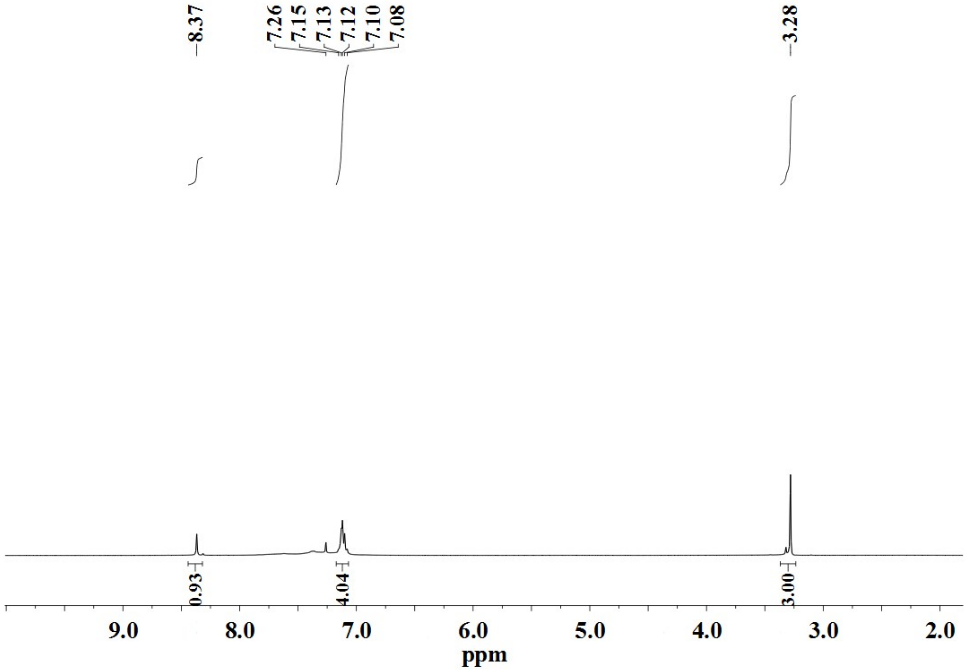

^{13}C NMR in $CDCl_3$